Growth and shape transition of small silicon self-interstitial clusters

Sangheon Lee and Gyeong S. Hwang*
Department of Chemical Engineering, University of Texas, Austin, Texas 78712, USA
(Received 12 January 2008; revised manuscript received 8 May 2008; published 14 July 2008)

The growth behavior of small self-interstitial clusters in crystalline Si is presented based on extensive combined Metropolis Monte Carlo, tight-binding molecular dynamics, and density-functional theory calculations. New stable structures for small interstitial clusters ($I_n, 5 \leq n \leq 16$) are determined, showing that the compact geometry appears favored when the cluster size is smaller than 10 atoms ($n < 10$). The fourfold-coordinated dodecainterstitial (I_{12}) structure with C_{2h} symmetry is identified to serve as an effective nucleation center for larger extended defects. This work provides the first theoretical support for earlier experiments which suggest a shape transition from compact to elongated structures around $n=10$.

DOI: 10.1103/PhysRevB.78.045204 PACS number(s): 61.72.J−

I. INTRODUCTION

There have been significant efforts to understand the fundamental behavior of Si interstitial defects created by bombardment with energetic dopant ions, due to their crucial role in defining ultrashallow *pn* junctions for ever smaller semiconductor device fabrication. Single Si interstitials are highly mobile even at room temperature.[1,2] Hence, in bulk Si, self-interstitials are likely to remain in the form of clusters or interstitial-impurity complexes. The formation and structure of rodlike {311} defects have been well characterized by high-resolution transmission electron microscopy (HRTEM).[3–5] In addition, a series of recent spectroscopy measurements[6–11] have evidenced existence of small compact self-interstitial clusters before they evolve into larger extended defects. In ultrashallow junction formation with low-energy implanted dopants, such small interstitial clusters are thought to be a main source for free interstitials responsible for dopant transient enhanced diffusion and agglomeration during postimplantation thermal treatment.[12–24] Hence, significant experimental and theoretical efforts[25–41] have been made to determine the structure and stability of small self-interstitial clusters as well as their growth to larger extended defects, yet still unclear.

Earlier inverse model studies[42,43] based on experimental observations of the spatial and temporal evolution of extended defect distribution in ion-implanted Si suggested the occurrence of structural transition between small compact clusters and larger extended defects when the cluster size is around 10 atoms. This prediction has been supported by a series of low-temperature photoluminescence (PL) studies[7,9,10] which show the signatures of small compact clusters of various sizes in ion-implanted Si upon short annealing. In addition, the PL measurements demonstrate changes in the spectra from multiple sharp peaks to broad but distinct signatures during prolonged annealing, ascribed to the shape evolution of self-interstitial clusters from compact to extended forms. While the empirical studies are rather limited to explicitly show the formation and atomic structure of small compact interstitial clusters, a few previous theoretical studies[30,33,40] also predicted the possibility that a chainlike, elongated tri-interstitial cluster may play a role for the compact-to-extended transition. Only a few small compact interstitial clusters ($I_n, n=2-4$) have been unequivocally identified by first-principles calculations.[27,28,33] At present, still the atomic structure and stability of larger compact clusters ($n \geq 5$) are uncertain due largely to the possible complexity in their geometries. The lack of information hampers revealing how small compact interstitial clusters grow to larger extended defects.

In this paper, we present the growth and structural evolution of Si self-interstitial clusters in Si based on a combination of continuous random network model based Metropolis Monte Carlo (CRN-MMC), tight-binding molecular dynamics (TBMD) and density-functional theory (DFT) calculations. We also discuss the growth of extended {311} defects from the small clusters.

II. CALCULATION METHODS

All atomic structures and energies reported herein were calculated using a plane-wave basis set pseudopotential method within the generalized gradient approximation of Perdew and Wang (GGA-PW91) (Ref. 44) to density-functional theory, as implemented in the well-established VIENNA AB INITIO SIMULATION PACKAGE (VASP).[45] Vanderbilt-type ultrasoft pseudopotentials[46] were used for core-electron interactions. Outer electron wave functions are expanded using a plane-wave basis set with a kinetic-energy cutoff of 160 eV. The Brillouin-zone sampling was performed using the $(2\times2\times2)$ Monkhorst-Pack mesh. We used the supercell approach for the defect calculations, with a fixed Si lattice constant of 5.460 Å as obtained from volume optimization. Special care was taken to ensure that each supercell size is large enough to accommodate a given interstitial cluster with no significant interaction with its periodic images. For each defect system, all atoms were fully relaxed using the conjugate gradient method until residual forces on constituent atoms become smaller than 5×10^{-2} eV/Å. For TBMD simulations, semiempirical potentials developed by Lenosky *et al.*[47] were used. A Keating (KT)-like valence bond model[48] was employed for CRN-MMC calculations. Within the Keating-like valence force model, the strain energy (E_{strain}) is given as

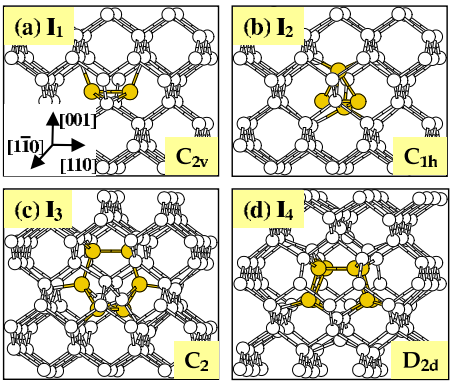

FIG. 1. (Color online) Ground state configurations for (a) single-, (b) di-, (c) tri-, and (d) tetrainterstitial defects in Si. Grey (gold) balls indicate more distorted atoms than the rest of the lattice atoms (in white). Corresponding defect symmetries are also indicated.

$$E_{\text{strain}} = \frac{1}{2}\sum_{i} k_b(b_i - b_0)^2 + \frac{1}{2}\sum_{i,j} k_\theta(\cos\,\boldsymbol{\theta}_{ij} - \cos\,\boldsymbol{\theta}_0)^2,$$

where b_i is the ith bond length and θ_{ij} is the bond angle between bonds i and j, and the equilibrium and force constants are b_o=2.365 Å, θ_0=109.5°, k_b=11.976 eV/Å^2 and k_θ=2.097 eV. A detailed description of KT parameter optimization can be found elsewhere.[41]

III. RESULTS AND DISUCSSION

A. Determination of small compact clusters

For the sake of comparison, we first determined the lowest-energy configurations of the single-, di-, tri-, and tetrainterstitial clusters in the neutral state. Our calculations show the ground-state ⟨110⟩-split, C_{1h}, C_2, and D_{2d} structures for I, I_2, I_3 and I_4, respectively, as also predicted by previous theoretical studies.[25,27,28,33] Here it is worth pointing out that our CRN-MMC calculations consistently predict the fourfold-coordinated C_2 and D_{2d} configurations for I_3 and I_4, respectively, as shown in Fig. 1, irregardless of the initial positions of interstitials so long as they are placed reasonably close to each other. This indicates the effectiveness of the CRN-MMC approach for determining fourfold defect structures in which all atoms have fourfold coordination.

Figure 2 shows minimum-energy structures which we have identified for I_5–I_{12} using a combination of CRN-MMC, TBMD, and DFT-GGA calculations. For each cluster size, we first constructed possible fourfold-coordinated structures using CRN-MMC simulations, followed by TBMD simulations at high temperatures (>1000 K) to check their thermal stability. Then, using DFT-GGA calculations we refined the geometries of the identified stable clusters, and compared their formation energies to determine the lowest-energy configuration among them. The combined approach has been proven to successfully determine minimum-energy configurations for Si self-interstitial clusters (I_n, $n \geq 3$), particularly when they prefer fourfold coordination.[41] Here, for

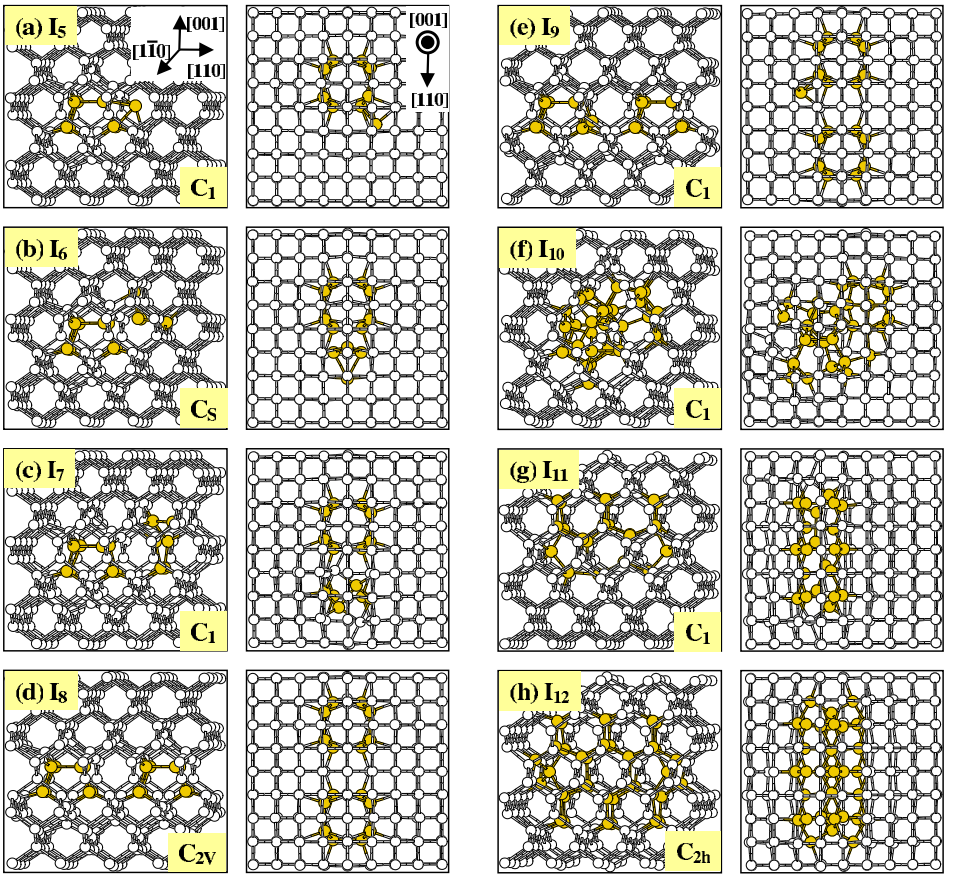

FIG. 2. (Color online) Predicted minimum-energy configurations for (a) penta-, (b) hexa-, (c) hepta-, (d) octa-, (e) ennea-, (f) deca-, (g) hendeca-, (h) dodecainterstitial defects in Si. For each defect, the left and right panels show two different views, as indicated. The symmetry of each defect is also indicated. Grey (gold) balls represent more distorted atoms than the rest of the lattice atoms (in white).

each cluster size we only present the lowest-energy state among several local minima identified from our extensive search. Other stable structures can be found elsewhere.[41]

Our results show that small interstitial clusters tend to favor compact structures, but the compact geometry is no longer favorable when the cluster size is greater than 10 interstitials. All atoms in the hendecainterstitial (I_{11}) [Fig. 2(g)] and dodecainterstitial (I_{12}) [Fig. 2(h)] clusters are fourfold coordinated, and they are elongated along the [110] direction. While the I_{11} cluster exhibits a somewhat asymmetric shape, the I_{12} structure is perfectly symmetric and less strained. The I_{12} structure has a mirror symmetry with respect to the (110) plane (perpendicular to the C_2 rotation axis along the [110] direction). Having four interstitials in each unit, the core part [Fig. 5(a)] is characterized by four adjacent six-membered rings surrounded by five-, six-, and seven-membered rings. The (110) edge atoms are also fourfold coordinated, and their bond angles and lengths vary from 98.8° to 128.2° and from 2.243 to 2.348 Å, respectively; insignificantly deviate from the equilibrium values of 109.5° and 2.365 Å in crystalline Si. The I_{12} formation energy is predicted to be 1.60 eV per interstitial, which is substantially lower than 3.80 eV for the ⟨110⟩-split single interstitial.

We also find that the octainterstitial (I_8) cluster (comprising two stable compact I_4 clusters) is very stable. For the lowest-energy I_8 structure, two intact I_4 structures are placed next to each other along the [110] direction, as shown in Fig. 2(d). The I_4-I_4 alignment with C_{2v} symmetry yields two eight-membered rings in the middle, which turns out to lower the induced strain, compared to two isolated I_4 clusters. While there is an energy variation with the I_4-I_4 alignment,[41] the predicted ground-state structure of I_8 is about 0.71 eV, more favorable than the case where two I_4 clusters are fully separated.

Due to the high thermal stability of the I_4 and I_8 structures, the pentainterstitial (I_5) [Fig. 2(a)] and enneainterstitial (I_9) clusters [Fig. 2(e)] favor the I_4+I and I_8+I geometries, respectively, where the additional single interstitial is located near their host I_4 or I_8 cluster. For the hexainterstitial (I_6) [Fig. 2(b)] and heptainterstitial (I_7) clusters [Fig. 2(c)], the combined I_4+I_2 and I_4+I_3 configurations appear energetically favored, with energy gains of 1.16 and 0.37 eV, respectively, over their fully separated counterparts, i.e., isolated I_2, I_3, and I_4 accordingly. Similarly, a stable I_8+I_2 configuration is identified for the decainterstitial (I_{10}) cluster, but turns out to be 0.36 eV less favorable than the stable fourfold-coordinate structure as shown in Fig. 2(f). Our calculations also predict the I_8+I_3 and I_8+I_4 structures to be 0.93 and 1.59 eV, less stable than the elongated, fourfold-coordinated I_{11} and I_{12} structures, respectively.

B. Compact-to-elongated transition

Figure 3 summarizes the calculated formation energies of small interstitial clusters. Here the formation energy per interstitial [$E_f(n)$] is given by:

$$E_f(n) = \{E(n+N) - (1+n/N) \times E(N)\}/n,$$

where $E(n+N)$ and $E(N)$ are the total energies of N-atom supercells with a n-interstitial cluster and with no defect,

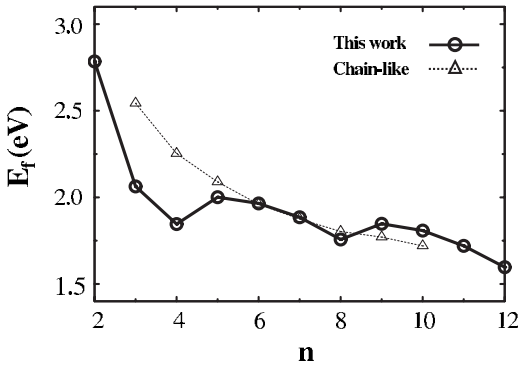

FIG. 3. Calculated formation energies per interstitial (E_f) of interstitial clusters shown in Figs. 1 and 2 (indicated as "This work") as well as chainlike elongated structures (indicated as "Chainlike") as a function of cluster size (n). For the chainlike case, the atomic structures from Ref. 30 were recalculated within DFT-GGA. To minimize possible interactions between a defect and its periodic images, we carefully evaluated the formation energies by changing the supercell size, i.e., $192+n$, $400+n$, $480+n$, $560+n$, and $672+n$ atom supercells, where n is the number of interstitials, for I_1-I_2, I_3-I_6, I_7-I_{10}, $I_{11}-I_{13}$, and $I_{14}-I_{16}$ clusters (This work), while $400+n$, $480+n$, $560+n$, and $640+n$ atom supercells, respectively, for I_3-I_4, I_5-I_6, I_7-I_8, and I_9-I_{10} (Chainlike).

respectively. The predicted values of 3.80, 2.79, 2.06, and 1.85 eV, respectively, for the I, I_2, I_3, and I_4 clusters are close to those from previous DFT-GGA calculations.[28,33] The predicted formation energies exhibit an oscillating trend as the cluster size varies, with strong minima at $n=4$ and 8, consistent with inverse modeling of experiments.[42,43]

When $n \leq 8$, as can seen in Fig. 3, the compact clusters are more stable than (or at least comparable to) the chainlike, elongated clusters (where a dumbbell interstitial is added to the previously relaxed cluster in the series, see Ref. 30). Our study also implies that the compact configurations would be hard to be transformed to the well-ordered chainlike configurations by fully destroying the stable fourfold I_4 structure. That is, our TBMD simulation at 1100 K shows that the I_4+I structure remains nearly unchanged for over 20 ps, whereas the I_3 compact cluster easily collapses when it captures an additional interstitial, which would further rearrange to the stable I_4 structure. This suggests that the stable I_4 and I_8 compact clusters would kinetically and/or thermodynamically hamper the formation of small chainlike clusters ($n \leq 10$). When $n > 10$, the elongated geometry becomes more stable than the compact shape, although it commonly consists of strained (110) edges which make it less favorable for smaller clusters. Our results are consistent with earlier experiments which suggested the occurrence of the compact to elongated transition at $n \approx 10$.[42,43]

Based on the calculation results, we discuss the nucleation and growth of large, extended defects. One possible mechanism may involve evolution from the fourfold compact to chainlike elongated structures at $n \approx 10$, followed by the capture of additional interstitials at (110) edges. Another growth mechanism may involve the elongated fourfold I_{11} and I_{12} clusters identified in this work. When $n > 10$, given the well-ordered structure with high thermal stability we hardly ex-

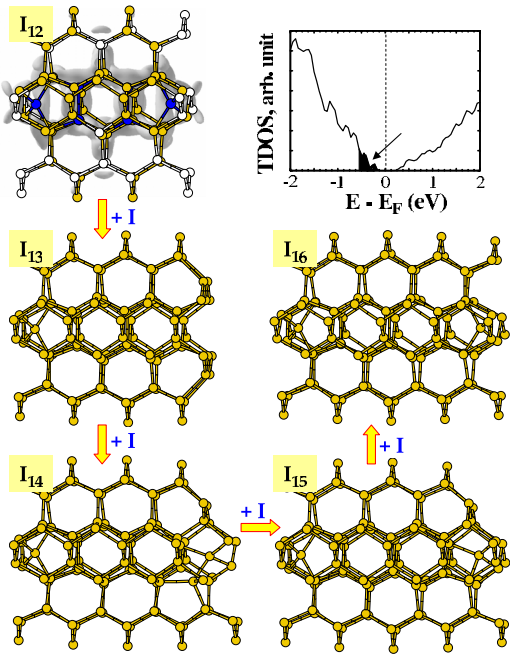

FIG. 4. (Color online) Minimum energy structures for I_{12}–I_{16} clusters, which illustrates a preferred growth along the [110] direction when $n>10$. The strain energy distribution around the I_{12} cluster is also shown at three different levels [high ($\geq$0.25 eV) =black (blue), medium (0.15–0.25 eV)=grey (gold), low ($<$0.15)=white, based on strain energy values from KT potential calculations], together with the isosurfaces of occupied orbitals near Fermi level (E_F), as indicated (shaded region) in the total density of state (TDOS) plot in the upper right panel. Here, the Fermi level is positioned at the top of the collection of electron energy levels.

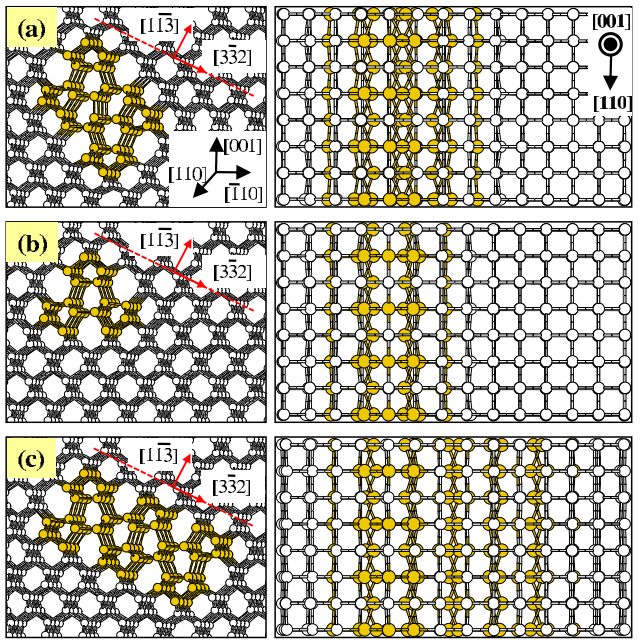

FIG. 5. (Color online) Three different defect core structures which are infinitely long in the ⟨110⟩ direction: (a) I_{12}-like (as shown for the fourfold I_{12} cluster identified in this work); (b) chainlike; (c) {311}. Grey (gold) balls indicate more distorted atoms than the rest of the lattice atoms (in white).

pect interconversion between the elongated fourfold-coordinated clusters (this work) and the chainlike ones.

Figure 4 (upper left panel) shows the local strain field around the fourfold I_{12} cluster and the isosurfaces of occupied orbitals near the Fermi level (as indicated in the DOS plot, upper right panel). The larger strain and the isosurface near the (110) edges indicate that they are more active than the (311) and (233) edges. Our TBMD simulations indeed demonstrate that an additional interstitial placed around the I_{12} cluster is preferentially captured at either (110) edge to form the fourfold I_{13} cluster. Figure 4 also shows the minimum-energy configurations for I_{14}, I_{15}, and I_{16} clusters (which have fourfold coordination), grown from the I_{12} cluster. The I_{13}, I_{14}, I_{15}, and I_{16} formation energies per interstitial are predicted to be 1.63, 1.63, 1.60, and 1.50 eV, respectively. Note that the I_{16} structure with C_{2h} symmetry is the extended form of I_{12} with an additional core unit in the [110] direction. By capturing additional interstitials, the interstitial defect further grows preferentially along the [110] direction. The result suggests that I_{12} can serve as an effective nucleation center for the growth of larger extended defects.

C. Growth to {311} extended defects

We finally look at the possible link of the small fourfold and chainlike clusters to extended defects with a {311} habit plane. In Fig. 5, we compare the I_{12}-like [(a), which represents the core structure of the fourfold I_{12} and I_{16} clusters identified in this work] and chainlike [(b)] core structures with a probable {311} core structure [(c)]. The {311} core consists of four six-membered rings in the middle layer and six five- and six seven-membered rings in the outer layers, as proposed by earlier studies.[49–51] Other {311} core configurations have also been predicted,[30,49–52] but somewhat similar to the structure considered here. For understanding the link between small clusters and {311} defects, hence it might be unnecessary to consider other possible {311} core configurations.

For each repeating unit, the I_{12}-like and {311} cores consist of four interstitials, while the chainlike one has two. Compared to the I_{12}-like core, the chainlike and {311} cores are twice longer in the ⟨110⟩ and ⟨233⟩ direction, respectively. The I_{12}-like and {311} cores exhibit a trace of {311}-habit plane when they are repeatedly placed along the ⟨233⟩ direction, but the chainlike one does not. In addition, transformation from the I_{12}-like to {311} core can be expected via structural relaxation in the ⟨233⟩ direction. However, it appears rather unlikely that the stable chainlike core would reconfigure to the {311} core, particularly considering its twice longer length in the ⟨110⟩ direction. That is, the chainlike→{311} reconfiguration requires that the chainlike structure should shrinks by half in the ⟨110⟩ direction while stretching to twice in the ⟨233⟩ direction, which is expected to hardly occur. The less dense {311} core is found to be more relaxed than the I_{12}-like core, as evidenced by its lower formation energy. The predicted formation energies of the {311}, I_{12}-like and chainlike cores are 1.11, 1.29, and 1.28 eV, respectively, provided the cores are infinitely long in the ⟨110⟩ direction, as shown in Fig. 5.

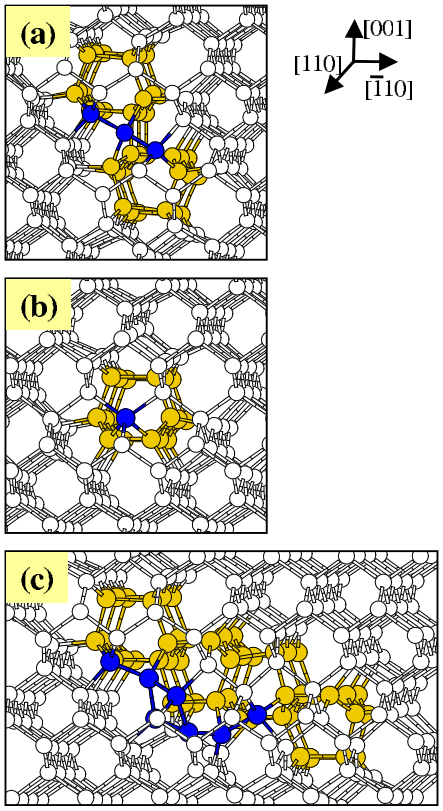

FIG. 6. (Color online) Minimum energy configurations for the (110) edges of (a) I_{12}-like, (b) chainlike, and (c) {311}-core containing clusters which are elongated along the [110] direction. Black (blue) balls indicate highly distorted atoms in the (110) edges, and gray (gold) balls represent more distorted atoms than the rest of the lattice atoms (in white).

For the sake of comparison, we also examine the relative stability of I_{12} and I_{16} clusters with the {311} core state, as the {311} core is energetically more stable than the I_{12}-like core. As shown in Fig. 6(c), the (110) edges can be fourfold coordinated, while each edge initially contains two dangling bonds. The fourfold coordination lowers the I_{12} formation energy by 1.1 eV, over the initial structure with dangling bonds. Using CRN-MMC simulations we also confirm that the fourfold edges can favorably be formed for larger clusters with the {311} core structure. However, we find that the edge structure is more strained than that with the I_{12}-like core [Fig. 6(a)]. For the I_{12} and I_{16} clusters, our calculations predict the {311}-core containing structures (with C_i symmetry) to be 1.4 and 0.8 eV, less favorable than the I_{12}-like core containing ones.

Figure 7 shows the relative stability of larger clusters with the I_{12}-like, chainlike, and {311} cores which we approximate using $E_f(n)=\{E_f^{\text{end}}+(n-n')E_f^c\}/n$, where E_f^{end} is the (110) edge energy, E_f^c is the core energy per interstitial for the infinitely elongated structure, and n' indicate the number of edge atoms. For the I_{12}-like and {311} cases, taking the core formation energies of $E_f^c=1.29$ and 1.11 eV, the corresponding edge energies are estimated to be $E_f^{\text{end}}=8.74$ and 11.62 eV, respectively, as fitted for I_{12} and I_{16}. Note that both cases have four edge atoms, i.e., $n'=4$. Similarly, for the chainlike

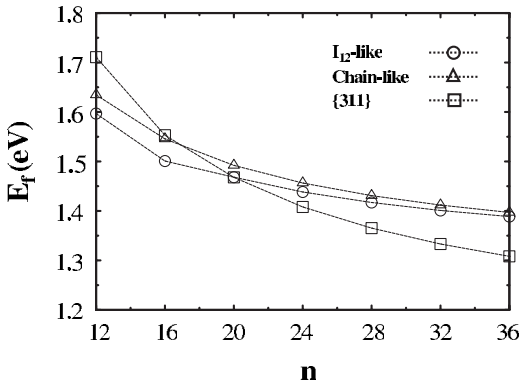

FIG. 7. Predicted formation energies per interstitial of I_{12}-like, chainlike, and {311} core containing interstitial clusters as a function of size (n) using $E_f(n)=\{E_f^{\text{end}}+(n-n')E_f^c\}/n$, where E_f^{end} is the (110) edge energy, E_f^c is the core energy per interstitial for the infinitely elongated structure, and n' is the number of edge atoms. The I_{12}-like represents the core structure of the fourfold I_{12} and I_{16} clusters identified in this work, the chainlike indicates the core structure that consists of dumbbell interstitials as also described in Fig. 3, and the {311} represents the {311} core structure in which all atoms are fourfold coordinated (see the text). Here, the edge energies were obtained by fitting to DFT-GGA values for the formation energies of smaller clusters, i.e., I_{12} and I_{16} for the I_{12}-like and {311} cases while I_8, I_9 and, I_{10} for the chainlike case. The predicted values are based on $E_f^c=1.29$, 1.28, and 1.11 eV and $E_f^{\text{end}}=8.74$, 6.83, and 11.62 eV for the I_{12}-like, chainlike and {311} cases, respectively, and $n'=4$ for the I_{12}-like and {311} cases and $n'=2$ for the chainlike case.

case we obtain $E_f^c=1.28$ eV and $E_f^{\text{end}}=6.83$ eV, where $n'=2$ (the chainlike structure has two edge atoms). According to the result, the {311} core structure becomes favored when the cluster size is greater than 20 atoms, below which the I_{12}-like core containing structure appears prevailing. This suggests a possible structural relaxation from the I_{12}-like to the {311} core state as the interstitial defect grows larger than $n\approx 20$ along the ⟨110⟩ direction.

We also construct an extended defect with a {311} habit plane by repeatedly placing the (110) elongated structure (with the {311} core) along the [233] direction. The predicted formation energy per interstitial is $E_f(\infty)=0.89$ eV, in good agreement with 0.7–1.4 eV as reported for extended {311} defects by previous studies.[53] A further investigation is underway to understand atomistic mechanisms regarding how extended {311} defects grow in the ⟨110⟩ and ⟨233⟩ directions.

IV. SUMMARY

We have determined stable compact geometries for small interstitial clusters ($n<10$), demonstrating that stable I_4 and I_8 compact clusters would kinetically or/and thermodynamically inhibit the formation of chainlike, elongated clusters. When the cluster size is greater than 10 atoms, our calculations show that elongated structures become more favorable energetically, although they commonly consist of highly strained (110) edges which make them less favorable for

smaller clusters. In particular, the newly discovered fourfold-coordinated I_{12} state is found to serve as an effective nucleation center for large extended defects. For the first time, this theoretical work provides explicit support for earlier experiments which suggested the occurrence of the compact to elongated transition at $n \approx 10$. In addition, the predicted formation energies per interstitial exhibit an oscillating trend with strong minima when $n=4$ and 8, while decreasing with cluster size in general, consistent with earlier inverse model studies based on experiments. While the fourfold I_{12}-like core is energetically less favorable than a typical {311} defect core, our theoretical study suggests the possible occurrence of further structural relaxation from the I_{12}-like to the {311} core state as the interstitial defect grows larger than $n \approx 20$ along the ⟨110⟩ direction.

ACKNOWLEDGMENTS

We acknowledge Semiconductor Research Corporation, National Science Foundation (CAREER-CTS-0449373), and Robert A. Welch Foundation (F-1535) for their financial support. We would also like to thank the Texas Advanced Computing Center for use of their computing resources.

*Author to whom correspondence should be addressed: gshwang@che.utexas.edu

[1] G. D. Watkins, Phys. Rev. B **12**, 5824 (1975).
[2] E. J. H. Collart, K. Weemers, N. E. B. Cowern, J. Politiek, P. H. L. Bancken, J. G. M. van Berkum, and D. J. Gravesteijn, Nucl. Instrum. Methods Phys. Res. B **139**, 98 (1998).
[3] S. Takeda, Jpn. J. Appl. Phys., Part 2 **30**, L639 (1991).
[4] A. Agarwal, T. E. Haynes, D. J. Eaglesham, H.-J. Gossmann, D. C. Jacobson, J. M. Poate, and Y. E. Erokhin, Appl. Phys. Lett. **70**, 3332 (1997).
[5] A. Claverie, B. Colombeau, B. de Mauduit, C. Bonafos, X. Hebras, C. Ben Assayag, and F. Cristiano, Appl. Phys. A: Mater. Sci. Process. **76**, 1025 (2003).
[6] J. L. Benton, S. Libertino, P. Kringhøj, D. J. Eaglesham, J. M. Poate, and S. Coffa, J. Appl. Phys. **82**, 120 (1997).
[7] D. C. Schmidt, B. G. Svensson, M. Seibt, C. Jagadish, and G. Davies, J. Appl. Phys. **88**, 2309 (2000).
[8] S. Libertino, S. Coffa, and J. L. Benton, Phys. Rev. B **63**, 195206 (2001).
[9] M. Nakamura and S. Murakami, J. Appl. Phys. **94**, 3075 (2003).
[10] P. K. Giri, Semicond. Sci. Technol. **20**, 638 (2005).
[11] D. Pierreux and A. Stesmans, Phys. Rev. B **71**, 115204 (2005).
[12] D. J. Eaglesham, P. A. Stolk, H.-J. Gossmann, and J. M. Poate, Appl. Phys. Lett. **65**, 2305 (1994).
[13] L. H. Zhang, K. S. Jones, P. H. Chi, and D. S. Simons, Appl. Phys. Lett. **67**, 2025 (1995).
[14] G. S. Hwang and W. A. Goddard, Phys. Rev. Lett. **89**, 055901 (2002).
[15] G. S. Hwang and W. A. Goddard, Appl. Phys. Lett. **83**, 1047 (2003).
[16] G. S. Hwang and W. A. Goddard, Appl. Phys. Lett. **83**, 3501 (2003).
[17] C. L. Kuo, W. Luo, and P. Clancy, Mol. Simul. **29**, 577 (2003).
[18] S. Solmi, M. Ferri, M. Bersani, D. Giubertoni, and V. Soncini, J. Appl. Phys. **94**, 4950 (2003).
[19] M. Y. L. Jung, R. Gunawan, R. D. Braatz, and E. G. Seebauer, J. Electrochem. Soc. **151**, G1 (2004).
[20] M. Y. L. Jung, C. T. M. Kwok, R. D. Braatz, and E. G. Seebauer, J. Appl. Phys. **97**, 063520 (2005).
[21] S. A. Harrison, T. F. Edgar, and G. S. Hwang, Appl. Phys. Lett. **87**, 231905 (2005).
[22] S. A. Harrison, T. F. Edgar, and G. S. Hwang, Phys. Rev. B **72**, 195414 (2005).
[23] S. A. Harrison, T. F. Edgar, and G. S. Hwang, Phys. Rev. B **74**, 195202 (2006).
[24] S. A. Harrison, T. F. Edgar, and G. S. Hwang, Electrochem. Solid-State Lett. **9**, G354 (2006).
[25] J. Zhu, T. Diaz dela Rubia, L. H. Yang, C. Mailhiot, and G. H. Gilmer, Phys. Rev. B **54**, 4741 (1996).
[26] P. B. Rasband, P. Clancy, and M. O. Thompson, J. Appl. Phys. **79**, 8998 (1996).
[27] N. Arai, S. Takeda, and M. Kohyama, Phys. Rev. Lett. **78**, 4265 (1997).
[28] J. Kim, F. Kirchhoff, W. G. Aulbur, J. W. Wilkins, F. S. Khan, and G. Kresse, Phys. Rev. Lett. **83**, 1990 (1999).
[29] B. J. Coomer, J. P. Goss, R. Jones, S. Öberg, and P. R. Briddon, Physica B (Amsterdam) **273-274**, 505 (1999).
[30] J. Kim, F. Kirchhoff, J. W. Wilkins, and F. S. Khan, Phys. Rev. Lett. **84**, 503 (2000).
[31] S. K. Estreicher, M. Gharaibeh, P. A. Fedders, and P. Ordejón, Phys. Rev. Lett. **86**, 1247 (2001).
[32] M. P. Chichkine and M. M. De Souza, Phys. Rev. B **66**, 045205 (2002).
[33] D. A. Richie, J. Kim, S. A. Barr, K. R. A. Hazzard, R. Hennig, and J. W. Wilkins, Phys. Rev. Lett. **92**, 045501 (2004).
[34] G. M. Lopez and V. Fiorentini, Phys. Rev. B **69**, 155206 (2004).
[35] L. A. Marqués, L. Pelaz, P. Castrillo, and J. Barbolla, Phys. Rev. B **71**, 085204 (2005).
[36] M. Cogoni, B. P. Uberuaga, A. F. Voter, and L. Colombo, Phys. Rev. B **71**, 121203(R) (2005).
[37] M. Posselt, F. Gao, and D. Zwicker, Phys. Rev. B **71**, 245202 (2005).
[38] A. Carvalho, R. Jones, J. Coutinho, and P. R. Briddon, Phys. Rev. B **72**, 155208 (2005).
[39] S. A. Centoni, B. Sadigh, G. H. Gilmer, T. J. Lenosky, T. Diaz dela Rubia, and C. B. Musgrave, Phys. Rev. B **72**, 195206 (2005).
[40] Y. A. Du, R. G. Hennig, T. J. Lenosky, and J. W. Wilkins, Eur. Phys. J. B **57**, 229 (2007).
[41] S. Lee and G. S. Hwang, Phys. Rev. B **77**, 085210 (2008).
[42] N. E. B. Cowern, G. Mannino, P. A. Stolk, F. Roozeboom, H. G. A. Huizing, J. G. M. van Berkum, F. Cristiano, A. Claverie, and M. Jaraíz, Phys. Rev. Lett. **82**, 4460 (1999).
[43] C. J. Ortiz, P. Pichler, T. Fühner, F. Cristiano, B. Colombeau, N. E. B. Cowern, and A. Claverie, J. Appl. Phys. **96**, 4866 (2004).
[44] J. P. Perdew and Y. Wang, Phys. Rev. B **45**, 13244 (1992).

[45] G. Kresse and J. Furthmuller, *VASP the Guide* (Vienna University of Technology, Vienna, 2001).
[46] D. Vanderbilt, Phys. Rev. B **41**, 7892 (1990).
[47] T. J. Lenosky, J. D. Kress, I. Kwon, A. F. Voter, B. Edwards, D. F. Richards, S. Yang, and J. B. Adams, Phys. Rev. B **55**, 1528 (1997).
[48] Y. Tu, J. Tersoff, G. Grinstein, and D. Vanderbilt, Phys. Rev. Lett. **81**, 4899 (1998).
[49] M. Kohyama and S. Takeda, Phys. Rev. B **46**, 12305 (1992).
[50] J. Kim, J. W. Wilkins, F. S. Khan, and A. Canning, Phys. Rev. B **55**, 16186 (1997).
[51] P. Alippi and L. Colombo, Phys. Rev. B **62**, 1815 (2000).
[52] J. P. Goss, T. A. G. Eberlein, R. Jones, N. Pinho, A. T. Blumenau, T. Frauenheim, P. R. Briddon, and S. Öberg, J. Phys.: Condens. Matter **14**, 12843 (2002).
[53] P. A. Stolk, H.-J. Gossmann, D. J. Eaglesham, D. C. Jacobson, C. S. Rafferty, G. H. Gilmer, M. Jaraíz, J. M. Poate, H. S. Luftman, and T. E. Haynes, J. Appl. Phys. **81**, 6031 (1997).